Research Networking Programmes

Short Visit Grant ☐ or Exchange Visit Grant ☒

(please tick the relevant box)

Scientific Report

Scientific report (one single document in WORD or PDF file) should be submitted online within one month of the event. It should not exceed eight A4 pages.

Dear Chair of the Steering Committee,
I'm truly sorry for the unsatisfactory file submitted to MeMoVolc. I have greatly appreciated your very useful comments to improve the quality of the report. I have now revised the report accordingly. In order to avoid future misunderstanding, I would like to highlight that in the website of the European Science Foundation it is recommended to use a template available online. This word file is protected and not editable. The document is arranged in 6 points. For each point there is a grey box in which you are forced to enter the text. This entered text cannot be formatted (e.g., apexes and subscripts, equation editor and symbols cannot be used) resulting highlighted in grey. Tables and figures cannot be included in the template. None of the information concerning researcher and host laboratory are requested in 6 points. As you have correctly observed, the format of this file and its content is strange causing that the final version of the report is basically unsatisfactory. It is also recommended in the template to do not exceed 4 pages in length. My previous report was 3 pages long and, according to your comments, it was succinct. However, any attempt to add more information in the text as well as add tables and figures summarizing results of 8 weeks of work will exceed the maximum number of 4 pages.
I have created a new file containing the new information requested. Clearly, this file is remarkably different from the template provided by the European Science Foundation. Since we fundamentally agree that this template is inappropriate to arrange the report, perhaps it should be removed from the website.

Thanks in advance for your time and your work.

Sincerely,
Silvio Mollo

Proposal Title: Magma dynamics feeding large volcanic eruptions: The case study of Campi Flegrei (Italy)

Application Reference N°: 4242

Researcher and affiliation: Silvio Mollo – Istituto Nazionale di Geofisica e Vulcanologia of Rome (Italy)

Host Laboratory and people involved: Institute of Geochemistry and Petrology at the ETH Zurich (Switzerland) – Prof. Olivier Bachmann, Chair in Volcanology and magmatic petrology

1) **Purpose of the visit**

The aim of this study is to better understand the crystallization conditions of one of the most important large caldera-forming eruption in Italy. The Campi Flegrei Volcanic Field (Campanian Region, Southern Italy) is an active volcanic region that covers an area of about 230 km^2. It experienced two cataclysmic caldera-forming eruptions which produced the Campanian Ignimbrite (39 ka) and the Neapolitan Yellow Tuff (15 ka). The eruption of the Campanian Ignimbrite, an unwelded to partially welded trachytic-phonolitic ignimbrite, is regarded as the dominant event in the history of the Campi Flegrei Volcanic Field with a minimum bulk volume of about 310 km^3 and initial areal distribution of about 30000 km^2 (Rolandi et al., 2003). The plumbing system of the Campi Flegrei Volcanic Field is still under debate and two main hypothesis have been evoked: (i) the presence of different magma batches evolved in separated magma chambers (Pabst et al., 2007) and (ii) the evolution of a unique shallower magmatic reservoir (Pappalardo and Mastrolorenzo, 2012). However, several geochemical, petrological and geophysical data are in favor of this second hypothesis. In fact, isotopic investigations have pointed out that magmas evolve in a compositionally zoned magma chamber (Pappalardo et al., 2002). Thermo-dynamical modeling and phase-equilibrium experiments have also demonstrated that shallower (250–150 MPa) crystal-poor felsic magmas with ~3 wt.% H_2O are supplied by a deeper crystal-rich mafic layer (Signorelli et al. 1999; Fowler et al. 2007; Fabbrizio and Carroll, 2008; Pappalardo et al., 2008). The presence of a unique shallow magmatic source is also supported by geophysical data underling the existence of a partial melting zone at 7–8 km depth where trachyphonolitic magmas originates by differentiation of a voluminous parent shoshonitic liquid (D'Antonio, 2011). This evolutionary process would lead to the formation of crystal mushes dominated by mafic phases (clinopyroxene and olivine) and significant amounts of melt directly correlated to the seismic wave velocity anomaly measured widespread beneath the caldera (Zollo et al., 2008). The plumbing system of the Campi Flegrei Volcanic Field appears to be comparable to other zoned chambers that fed voluminous explosive eruptions in the world (e.g., Blake, 1981; Blake and Ivey, 1986; Wallace et al., 1999; Wark et al., 2007). During my visit at ETH, I have analysed the compositions of crystals and glasses in some products of the Flegrei Volcanic Field. By means of activity models, I have tested for equilibrium between crystals and glasses. Then, equilibrium data have been used as input data for thermometers and hygrometers to estimate the crystallization temperatures and water contents of magmas. In particular, using equilibrium K-feldspar-liquid pairs, I have calibrated a new hygrometer allowing to accurately predict the water dissolved in magmas immediately prior to eruptions.

2) <u>Description of the work carried out during the visit</u>

I have performed microprobe analyses of clinopyroxenes, feldspars and glasses found in seven products from the Campi Flegrei Volcanic Field (Table 1). For glasses, a slightly defocused electron beam with a size of 3 μm was used with a counting time of 5 s on background and 15 s on peak. For crystals, the beam size was 1 μm with a counting time of 20 and 10 s on peaks and background, respectively. The following standards have been adopted for the various chemical elements: jadeite (Si and Na), corundum (Al), forsterite (Mg), andradite (Fe), rutile (Ti), orthoclase (K), barite (Ba), apatite (P), spessartine (Mn) and chromite (Cr). Sodium and potassium were analyzed first to prevent alkali ion migration effects. The precision of the microprobe was measured through the analysis of well-characterized synthetic oxides and minerals. Data quality was ensured by analyzing these test materials as unknowns. Based on counting statistics, analytical uncertainties relative to their reported concentrations have indicated that precision was better than 5% for all cations. The products are trachytic to phonolitic in composition and constrain the large caldera-forming eruption of the Campanian Ignimbrite (hereafter named CI). Coherently with their relative stratigraphic position, these samples have been grouped as pre-CI, CI and post-CI. In order to retrieve the crystallization parameters of Campi Flegrei magmas, clinopyroxene- and feldspar-melt equilibria were studied by means of thermometric and hygrometric models. Results were compared with those reported by previous studies in order to better understand magma dynamics at Campi Flegrei.

3) <u>Description of the main results obtained</u>

The pre-eruptive temperatures of our products were estimated through one of the most recent clinopyroxene-based thermometer calibrated by Masotta et al. (2013). This is a pressure-independent model (Eqn. Talk2012) with a very low uncertainty (±18 °C) due to regression analyses of experimental compositions specific to alkaline differentiated magmas. As input data, we have selected clinopyroxene rim and co-existing liquids. To ascertain whether the clinopyroxene-liquid pairs were in equilibrium at the time of crystallization, we have used the Fe-Mg exchange reaction [$^{cpx\text{-}liquid}Kd_{Fe\text{-}Mg} = (Fe^{cpx}/Fe^{liquid}) \times (Mg^{liquid}/Mg^{cpx})$] modeled by Putirka (2008). With the exception of a number of data mostly from the CI sample, measured $^{cpx\text{-}liquid}Kd_{Fe\text{-}Mg}$ (0.24-0.27) closely match with both the equilibrium ranges of 0.27±0.03 and 0.28±0.08 indicated by Putirka et al. (2003) and Putirka (2008), respectively (Fig. 1). As a further test for equilibrium, we have adopted the model of Mollo et al. (2013) based on the difference (Δ) between diopside + hedenbergite (DiHd) components predicted for clinopyroxene via regression analyses of

clinopyroxene-liquid pairs in equilibrium conditions, with those measured in the analyzed crystals. Considering that ΔDiHd equals to zero at thermodynamic equilibrium, we have assumed as near-equilibrium crystallization conditions values ≤0.02. The plot of Fig. 2 reveals strong disequilibrium conditions for the majority of clinopyroxene-liquid pairs found in CI product, coherently with results from Fe-Mg exchange reaction (Fig. 1). After the screening of disequilibrium data, we used equation Eqn. Talk2012 to estimate the thermal paths of magmas feeding eruptions. Our predictions yield crystallization temperatures of 860-970 °C, 750-1156 °C, and 770-965 °C for pre-CI, CI and post-CI samples, respectively (Fig. 3); notably, the crystallization of clinopyroxene in CI magma occurs over a wider thermal path relative to other samples (see discussion below). To measure the water content of these magmas, we have calibrated a K-feldspar–liquid hygrometer specific for trachytic to phonolitic compositions. The calibration dataset consists of laboratory experiments conducted by previous authors at 0.05-0.3 GPa, 725-950 °C, 2.7-9.5 wt.% H_2O and QFM-NNO+1.5 buffers (i.e., Fabbrizio and Carrol 2008; Andujar et al. 2008, 2010; Andujar and Scaillet 2012; Masotta et al., 2013) and MELTS (Ghiorso and Sack, 1995) numerical simulations performed at 0.15-0.3 GPa, 1020-803 °C, 0.0-8.0 wt.% H_2O and QFM-NNO+0.5 buffering conditions. We stress out that there is a fairly agreement between phase relationships and compositions predicted by MELTS and those observed in natural and experimental alkaline differentiated products (e.g., Fowler et al., 2007; Masotta et al., 2010). A number of regression analyses have been performed prior to derive a new and more precise hygrometer. Each variable was checked using partial-regression leverage plots to ensure that a given model parameter is significant and so explained by more than just one or a few potentially aberrant data. The melt-water content was plotted versus the cation fraction of liquids and K-feldspars in order to capture the regression variables with the highest degrees of correlation. Then, more complex terms, e.g., $Mg\#^{liq} = [MgO/(MgO + FeO_{tot})]^{liq}$ and the ratio of $[Si/(K + Na + Ca)]^{liq}$, were considered to improve H_2O prediction. Importantly, our new regression models were developed including only those parameters that closely describe the variance of the dataset (cf. Putirka et al. 1999), whereas all parameters producing data overfitting were removed from the regression analysis (Jefferys and Berger 1992; Ratkowsky 1990). Doing this, we have determined the minimum number of parameters that are required to explain observed variability, thus calibrating the following regression model (Fig. 4a):

Eqn. Kfs1

$$H_2O(wt.\%) = 22.226 - 1.993\times10^{-2}T(°C) + 1.714\ln\left[\frac{Si}{(K+Na+Ca)}\right]^{liq}$$
$$- 0.117\ln\left(An^{Kfs}\right) - 534.319Ti^{liq} - 1.357Mg\#^{liq}$$

($R^2 = 0.90$; SEE = 0.69)

In order to verify the accuracy of our hygrometers, we have used as test data K-feldspar–liquid pairs not included into the calibration dataset. Results show that equation Kfs1 successfully reproduces melt-water contents for the test dataset according to the high correlation coefficient and low standard error of estimate (Fig. 4b). This finding ensures that there are no systematic overestimates or underestimates due to mis-calibrations, as well as that the type and number of used model parameters avoid overfitting. One of the crucial issue in using mineral-liquid activity models is whether the crystal phases are in equilibrium with the coexisting liquids. In the light of previous results of Putirka (2008), we have examined the behaviour of both Ab-An and Or-Ab exchanges for K-feldspar–liquid pairs from our calibration dataset. The proportions of Ab-An-Or in K-feldspar led to no significant regression coefficients for $^{kfs\text{-}liq}Kd_{Ab\text{-}An}$, whereas a best-fitting equation was derived for $^{kfs\text{-}liq}Kd_{Or\text{-}An}$ (Fig. 5a):

Eqn. Kfs2

$$^{kfs-liq}Kd_{Or-Ab}\times100 = 0.479 + \frac{0.223\times10^3T(°C)}{\left[\frac{Or}{(Ab+An)}\right]^{liq}} + \frac{0.117\times10^3T(°C)}{\ln\left[\frac{Or}{(Ab+An)}\right]^{Kfs}}$$

($R^2 = 0.94$; SEE = 0.06)

The equation Kfs2 is a T-sensitive model like those proposed for $^{cpx\text{-}liq}Kd_{Fe\text{-}Mg}$ by Putirka (2008) and Masotta et al. (2003) but it also accounts for the equilibrium proportion between Or and Ab + An in K-feldspar and coexisting liquid over the effect of temperature. Following the same strategy adopted for hygrometers, we have verified the accuracy of this model using test data not included into the calibration dataset. The equation Kfs2 successfully captures most of the equilibrium K-feldspar-liquid pairs, as indicated by the good correlation coefficient ($R^2 = 0.93$) and standard error of estimate (SEE = 0.04) of the linear regression showed in Fig. 5b. Using equation Kfs2 we have tested for equilibrium natural pre-CI, CI and post-CI samples assuming as reliable K-feldspar and liquid compositions those plotting within 10 % of the one-to-one line (Fig. 6a). A number of CI data exhibit strong deviations between predicted and measured $^{kfs\text{-}liq}Kd_{Or\text{-}An}$ paralleling results from Fe-Mg exchange between clinopyroxene and liquid (Fig. 1) and difference between predicted and observed components in clinopyroxene (Fig. 2). Much lower degrees of disequilibrium are observed for post-CI compositions and near-equilibrium conditions are recovered for pre-CI products. After the screening of disequilibrium data, we used equation Kfs1 to estimate the melt-water contents at the optimum K-feldspar crystallization conditions (0.1 GPa and 825 °C) determined for magmas of Campi Flegrei Volcanic Field (Fowler et al., 2007). Our predictions yield comparable water contents for pre-CI and CI eruptions ranging from 3.5 and 8 wt.% (Fig. 6b); whereas, lower concentrations of 4.2-6.4 wt.% H_2O are measured for post-CI product. These estimates are consistent with a number of previous melt inclusion data measuring water concentrations of 1.3-3.1 and 3.3-7.4 wt.% for primitive and more evolved magmas, respectively (Cecchetti et al., 2001, 2005; Signorelli et al., 2001; Cannatelli et al., 2007; Mangiacapra et al., 2008; Esposito et al., 2011). We stress out that CI represents the major explosive event of the Mediterranean region in the last 200000 years erupting 145 km^3 of more or less differentiated trachytic magmas by sequential tapping of a compositionally zoned magmatic reservoir (Di Girolamo and Morra 1987; Cornell et al. 1993; Civetta et al. 1997; Signorelli et al. 1999). The very high melt-water contents measured for pre-CI and CI products (Fig. 8b) are due to water-saturated conditions prior to cataclysmic caldera-forming eruption. In fact, thermo-dynamical models (Pappalardo et al., 2008) and experiments (Fabbrizio and Carroll, 2008) have demonstrated that CI magma was mainly water-saturated and capable of generating critical conditions of over-pressurisation in the chamber. In this regard, the lower melt-water contents recorded by post-CI, product are the consequence of eruption-induced decompression events: as pressure is released during caldera collapse, the volatile saturation level will drop deeper in the magmatic column, depleting magmas in volatiles (Bachmann et al., 2011 and references therein). The different amount of dissolved water in primitive CI melt inclusions (<3 wt.% H_2O) and matrix glasses (<1 wt.% H_2O) indicate strong magma degassing during ascent from the magma chamber toward the surface with remarkable gas loss at shallow depths (1.1-1.6 km) and in the conduit (<0.8 km) (Pappalardo and Mastrolorenzo, 2012 and references therein). Dynamic crystallization conditions for CI magma are revealed by the number of disequilibrium data captured by models based on crystal-liquid exchange reactions, i.e., $^{cpx\text{-}liquid}Kd_{Fe\text{-}Mg}$ (Fig. 1), ΔDiHd (Fig. 2) and $^{kfs\text{-}liq}Kd_{Or\text{-}An}$ (Fig. 6a), as well as by the wide range of clinopyroxene crystallization temperature (Fig. 3) and melt-water content (Fig. 6b). Despite the lack of melt inclusions in the more evolved CI products precludes any direct estimation of the water content (Signorelli et al., 2001), the empirical model of Moore et al. (1998) predicts that the solubility of water in magma increases from 4.2 to 6.2 wt.% as the temperature decreases from 1150 to 850 °C at 0.15 GPa. MELTS runs performed by Fowler et al. (2007) corroborates these predictions, underlining that CI magma is water-saturated at 1127 °C and 4.4 wt.% H_2O, and that the dissolved water content continues to increase at the rate of 1 wt.% H_2O per 50 °C as heat is extracted and crystals precipitate. However, while water-poor primitive melt inclusions are entrapped in olivine and clinopyroxene at relative high temperatures (1230 and 1160 °C, respectively), K-feldspar saturates CI magma at the late stage of differentiation (880 °C) under water-rich conditions (Fowler et al., 2007). Additionally, the lower crystallization temperature of K-feldspar coincides with a pseudo-invariant point where the fraction of melt remaining in the system abruptly decreases from 0.5 to <0.1 leading to changes in the composition, properties (density, dissolved water content), and physical state (viscosity, volume fraction fluid) of melt, possibly setting the stage for highly explosive eruptions (Fowler et al., 2007). This basically points out that our new K-feldspar–liquid hygrometers has paramount implications for volcanic hazard since they permits to predict the amounts of water dissolved in alkaline differentiated magmas immediately prior to the onset of eruptions or at syn-eruptive conditions whether degassing-induced crystallization of K-feldspar occurs at shallow depths or in the conduit.

4) <u>Future collaboration with host institution (if applicable)</u>

There is an ongoing three-years collaboration between the INGV (Rome) and ETH (Zurich) on a project funded by Swiss National Science Foundation to improve our understanding of magma reservoirs feeding large volcanic eruptions.

5) **Projected publications / articles resulting or to result from the grant (ESF must be acknowledged in publications resulting from the grantee's work in relation with the grant)**

There is a draft of a manuscript dealing with a new hygrometer specific to alkaline differentiated magmas at Campi Flegrei.

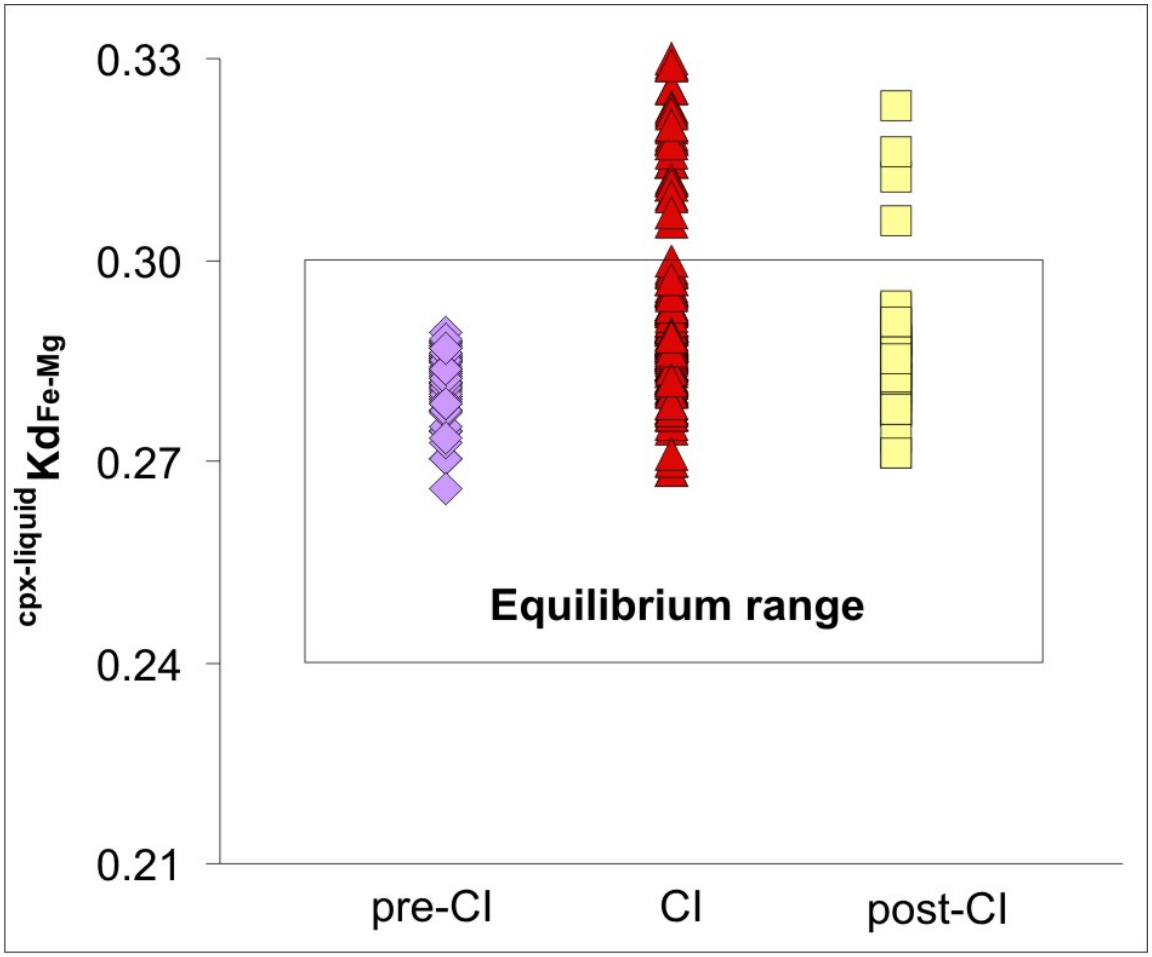

Fig.1. Test for equilibrium based on Fe-Mg exchange reaction between clinopyroxene and liquid [$^{cpx\text{-}liquid}Kd_{Fe\text{-}Mg} = (Fe^{cpx}/Fe^{liquid}) \times (Mg^{liquid}/Mg^{cpx})$] modeled by Putirka (2008). With the exception of a number of data mostly from the CI sample, measured $^{cpx\text{-}liquid}Kd_{Fe\text{-}Mg}$ (0.24-0.27) closely match with both the equilibrium ranges of 0.27±0.03 and 0.28±0.08 indicated by Putirka et al. (2003) and Putirka (2008), respectively.

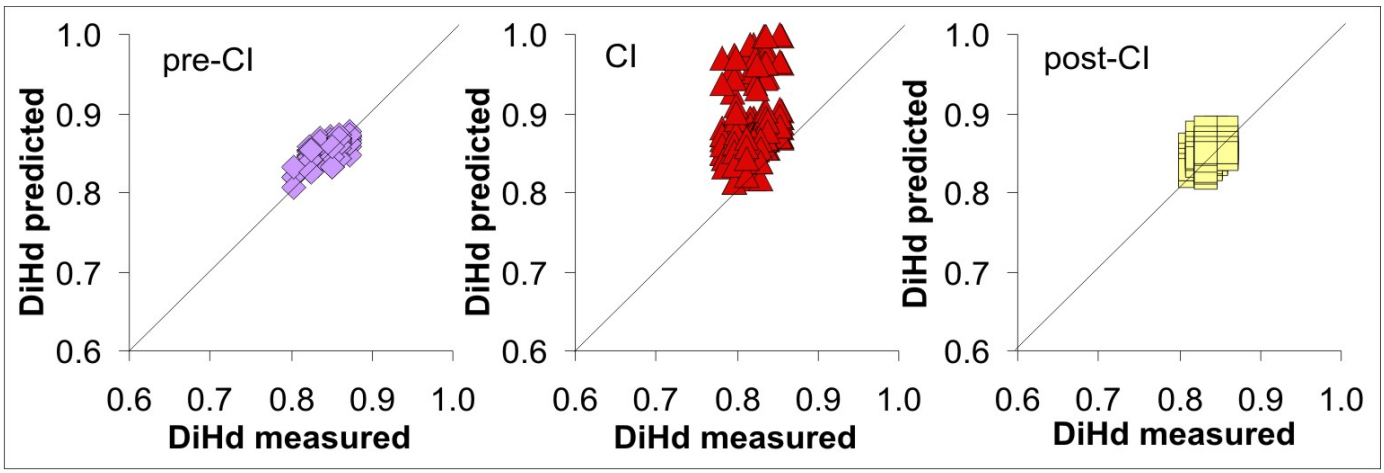

Fig. 2. Test for equilibrium based on the model of Mollo et al. (2013). The difference (Δ) between diopside + hedenbergite (DiHd) components predicted for clinopyroxene via regression analyses of clinopyroxene-liquid pairs in equilibrium conditions, with those measured in the analyzed crystals. Considering that ΔDiHd equals to zero at thermodynamic equilibrium, we have assumed as near-equilibrium crystallization conditions values ≤0.02. The plot reveals strong disequilibrium conditions for the majority of clinopyroxene-liquid pairs found in CI product, coherently with results from Fe-Mg exchange reaction (Fig. 1).

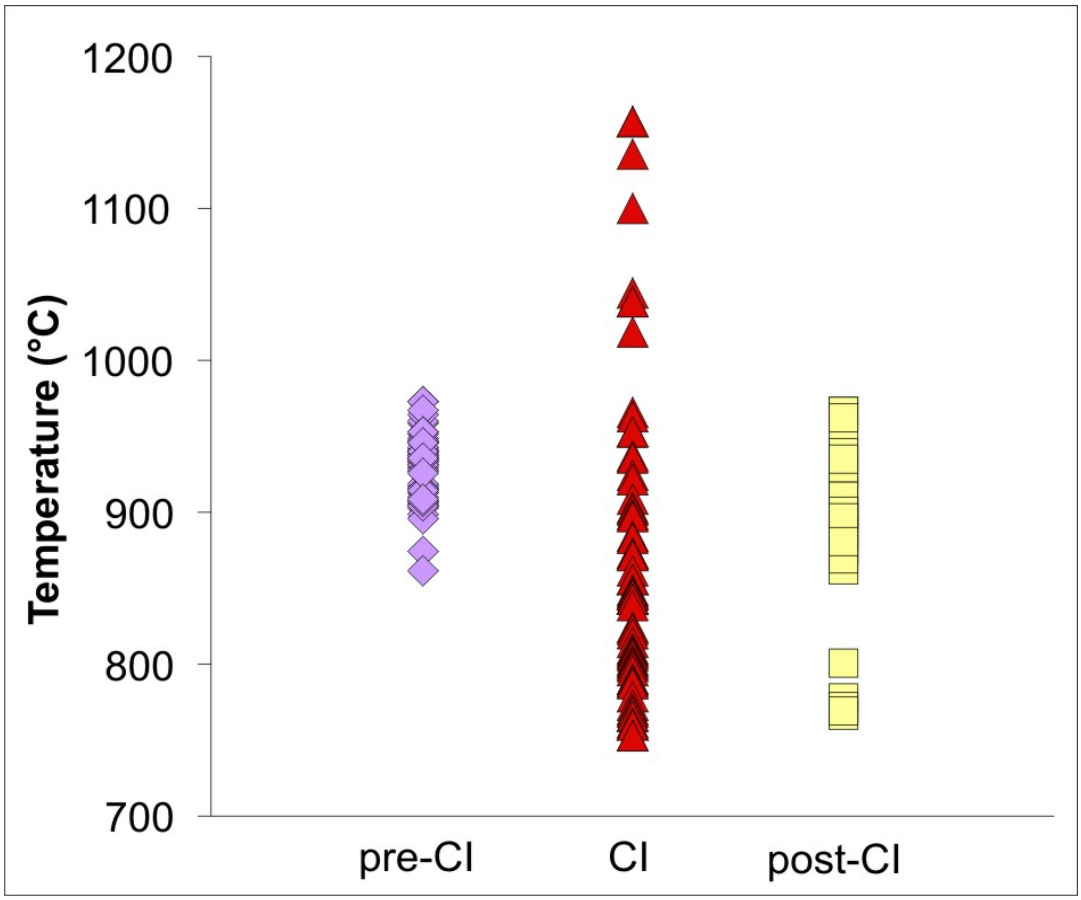

Fig. 3. Estimates of clinopyroxene crystallization temperatures conducted with Eqn. Talk2012 by Masotta et al., 2013. Our predictions yield crystallization temperatures of 860-970 °C, 750-1156 °C, and 770-965 °C for pre-CI, CI and post-CI samples, respectively; notably, the crystallization of clinopyroxene in CI magma occurs over a wider thermal path relative to other samples.

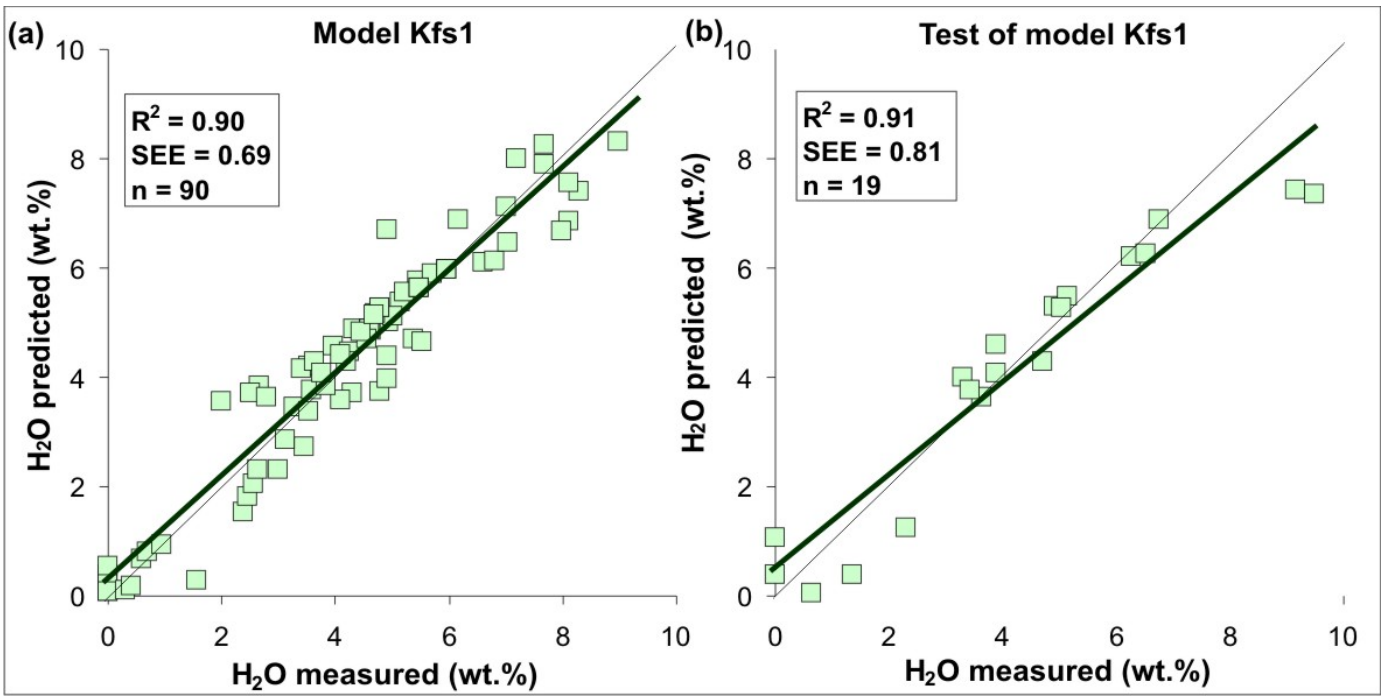

Fig. 4. Calibration of a new K-feldspar-liquid hygrometer specific to magmas of Campi Flegrei Volcanic Field (a); the calibration dataset consists of laboratory experiments conducted by previous authors at 0.05-0.3 GPa, 725-950 °C, 2.7-9.5 wt.% H_2O and QFM-NNO+1.5 buffers (i.e., Fabbrizio and Carrol 2008; Andujar et al. 2008, 2010; Andujar and Scaillet 2012; Masotta et al., 2013) and MELTS (Ghiorso and Sack, 1995) numerical simulations performed at 0.15-0.3 GPa, 1020-803 °C, 0.0-8.0 wt.% H_2O and QFM-NNO+0.5 buffering conditions. Test of model Kfs1 based on K-feldspar-liquid pairs not included in the calibration dataset (b).

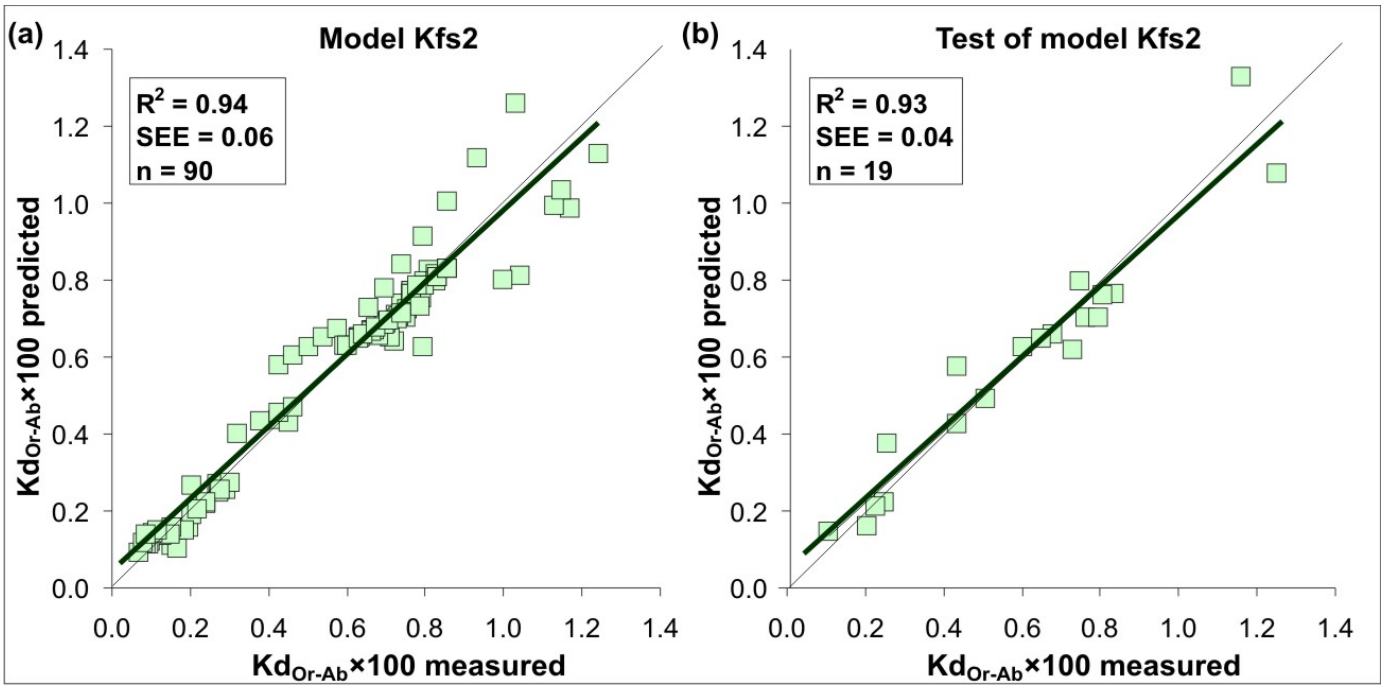

Fig. 5. Calibration of Kfs2 model for equilibrium based on Or-Ab exchange between K-feldspar and liquid (a). Test of model Kfs2 via regression analysis of data non included in the calibration dataset (b).

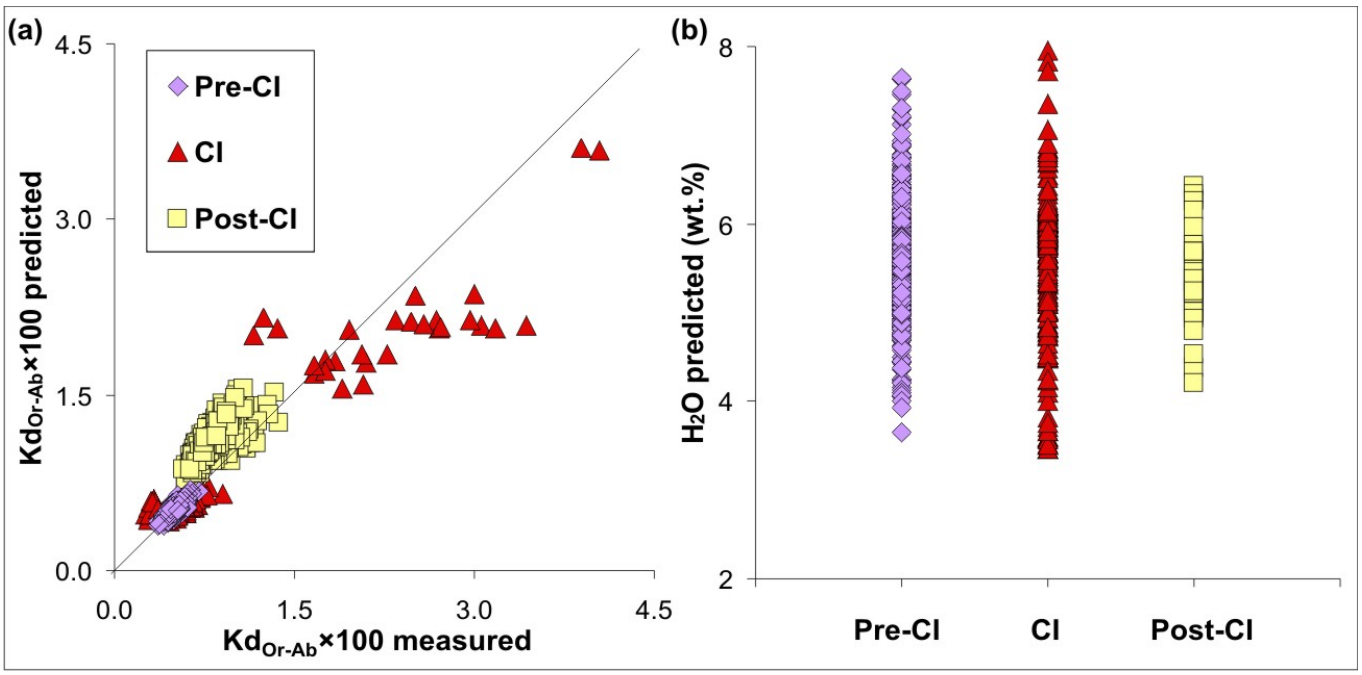

Fig. 6. Using equation Kfs2 we have tested for equilibrium natural pre-CI, CI and post-CI samples assuming as reliable K-feldspar and liquid compositions those plotting within 10 % of the one-to-one line (a); a number of CI data exhibit strong deviations between predicted and measured $^{kfs-liq}Kd_{Or-An}$. After the screening of disequilibrium data, we used equation Kfs1 to estimate the melt-water contents at the optimum K-feldspar crystallization conditions (0.1 GPa and 825 °C) determined for magmas of Campi Flegrei Volcanic Field (b); our predictions yield comparable water contents for pre-CI and CI eruptions ranging from 3.5 and 8 wt.%, whereas lower concentrations of 4.2-6.4 wt.% H_2O are measured for post-CI product.

Table 1. Representative analyses of clinopyroxenes, K-feldspars and glasses found in pre-CI, CI and post-CI products. CI: Campanian Ignimbrite.

SiO_2	TiO_2	Al_2O3	FeO_{tot}	MnO	MgO	CaO	Na_2O	K_2O	P_2O_5	Tot
Liquid (Glass) Compositions - in Weight Percent										
Pre-CI samples										
62.81	1.01	17.67	2.75	0.18	0.72	1.97	5.87	6.86	0.00	100.00
61.07	0.37	17.82	3.25	0.27	0.68	2.27	6.76	7.41	0.00	100.00
61.80	0.50	18.89	2.43	0.17	0.84	2.21	5.58	7.57	0.00	100.00
61.03	0.15	18.74	3.22	0.14	0.66	2.09	6.40	7.37	0.00	100.00
62.03	0.29	18.62	3.30	0.40	0.43	2.10	5.72	7.07	0.00	100.00
61.73	0.19	18.21	3.94	0.22	0.51	1.85	5.97	7.14	0.00	100.00
60.90	0.62	19.03	3.35	0.00	0.62	1.78	6.02	7.32	0.00	100.00
61.25	0.54	17.34	3.06	0.00	0.74	2.59	6.92	7.56	0.00	100.00
61.53	0.54	18.43	3.54	0.16	0.40	1.88	5.76	7.38	0.00	100.00
CI samples										
61.18	0.40	16.44	3.97	0.66	1.05	2.47	5.67	8.15	0.00	100.00
56.51	0.52	15.27	6.50	1.65	2.36	5.56	6.94	4.71	0.00	100.00
62.11	0.40	20.98	0.45	0.21	0.59	1.21	7.35	6.70	0.00	100.00
58.42	0.88	15.51	2.94	0.33	7.63	1.28	3.08	9.90	0.03	100.00
61.18	0.40	16.44	3.97	0.66	1.05	2.47	5.67	8.15	0.00	100.00
56.51	0.52	15.27	6.50	1.65	2.36	5.56	6.94	4.71	0.00	100.00
61.18	0.40	16.44	3.97	0.66	1.05	2.47	5.67	8.15	0.00	100.00
56.51	0.52	15.27	6.50	1.65	2.36	5.56	6.94	4.71	0.00	100.00
58.84	0.46	15.86	5.24	1.16	1.70	4.01	6.30	6.43	0.00	100.00
Post-CI samples										
64.63	0.07	20.73	0.59	0.00	0.07	2.45	6.39	5.08	0.00	100.00
66.04	0.25	18.35	2.04	0.15	0.10	1.41	5.83	5.83	0.00	100.00
65.54	0.26	18.63	1.75	0.23	0.05	1.10	5.77	6.68	0.00	100.00
67.01	0.34	17.09	1.81	0.07	0.02	1.26	6.03	6.37	0.00	100.00
64.97	0.27	19.23	2.42	0.22	0.11	1.41	5.71	5.58	0.08	100.00
64.43	0.22	17.75	2.00	0.42	0.56	1.82	6.31	6.50	0.00	100.00
64.37	0.01	17.32	2.60	0.73	0.40	1.84	5.97	6.73	0.03	100.00
64.30	0.46	16.93	2.44	0.00	0.37	2.15	6.15	7.01	0.20	100.00
65.37	0.39	15.78	2.92	0.36	0.45	1.74	6.85	6.15	0.00	100.00
64.77	0.50	17.66	2.83	0.25	0.34	1.29	5.97	6.39	0.00	100.00
Liquid (Glass) Compositions - in Weight Percent										
Pre-CI samples										
62.81	1.01	17.67	2.75	0.18	0.72	1.97	5.87	6.86	0.18	100.00
61.07	0.37	17.82	3.25	0.27	0.68	2.27	6.76	7.41	0.25	100.00
62.81	1.01	17.67	2.75	0.18	0.72	1.97	5.87	6.86	0.36	100.00
61.80	0.50	18.89	2.43	0.17	0.84	2.21	5.58	7.57	0.00	100.00
61.03	0.15	18.74	3.22	0.14	0.66	2.09	6.40	7.37	0.04	100.00
61.73	0.19	18.21	3.94	0.22	0.51	1.85	5.97	7.14	0.36	100.00
60.90	0.62	19.03	3.35	0.00	0.62	1.78	6.02	7.32	0.00	100.00
61.25	0.54	17.34	3.06	0.00	0.74	2.59	6.92	7.56	0.39	100.00
61.53	0.54	18.43	3.54	0.16	0.40	1.88	5.76	7.38	0.00	100.00
61.43	0.45	18.45	2.98	0.59	0.43	1.85	6.78	7.05	0.00	100.00
CI samples										
61.18	0.40	16.44	3.97	0.66	1.05	2.47	5.67	8.15	0.00	100.00
56.51	0.52	15.27	6.50	1.65	2.36	5.56	6.94	4.71	0.00	100.00
62.11	0.40	20.98	0.45	0.21	0.59	1.21	7.35	6.70	0.00	100.00
58.42	0.88	15.51	2.94	0.33	7.63	1.28	3.08	9.90	0.03	100.00
61.18	0.40	16.44	3.97	0.66	1.05	2.47	5.67	8.15	0.00	100.00
65.04	0.26	18.36	0.31	0.20	0.01	0.80	5.97	9.05	0.00	100.00
64.85	0.03	19.26	0.69	0.41	0.02	1.18	6.88	6.53	0.13	100.00
64.24	0.15	19.30	0.82	0.08	0.56	1.49	5.68	7.66	0.00	100.00
64.73	0.43	18.50	0.94	0.00	0.24	0.72	5.07	9.40	0.00	100.00
64.60	0.52	18.95	0.56	0.00	0.66	0.71	5.87	7.75	0.37	100.00
Post-CI samples										
60.90	0.43	18.67	2.86	0.10	0.71	2.12	4.87	9.22	0.12	100.00
60.73	0.71	18.58	3.48	0.00	0.54	2.57	4.85	8.54	0.00	100.00

SiO_2	TiO_2	Al_2O3	FeO_{tot}	MnO	MgO	CaO	Na_2O	K_2O	Tot
Clinopyroxene Compositions - in Weight Percent									
Pre-CI samples									
50.39	0.66	2.85	10.00	0.48	13.64	21.25	0.89	0.00	100.16
51.71	0.35	2.52	8.64	0.53	13.91	22.38	0.38	0.00	100.42
50.94	0.85	2.46	9.49	0.58	13.05	21.34	0.72	0.00	99.43
50.32	0.68	2.43	9.63	1.45	12.67	22.09	0.66	0.00	99.93
49.47	1.14	2.47	10.98	0.83	11.92	21.53	0.69	0.00	99.03
51.02	0.74	2.56	9.82	1.09	12.52	21.71	0.69	0.00	100.15
48.58	0.93	3.12	10.54	1.03	11.84	22.79	0.27	0.00	99.10
49.24	1.05	3.22	10.34	0.75	12.58	21.78	0.72	0.00	99.68
49.31	0.59	3.97	8.63	0.51	13.29	23.28	0.19	0.00	99.77
CI samples									
48.92	0.78	2.54	11.49	1.22	12.85	20.35	0.49	0.00	98.64
52.44	0.87	2.17	2.97	0.34	18.17	21.89	0.19	0.00	99.04
51.22	0.49	3.76	4.38	0.46	17.16	22.24	0.09	0.00	99.80
51.91	0.12	2.97	3.85	0.00	17.84	22.65	0.07	0.00	99.41
50.23	0.65	2.64	10.13	0.48	12.39	21.52	0.86	0.00	98.90
52.71	0.56	3.08	4.95	0.00	16.90	22.46	0.08	0.00	100.74
50.32	0.77	2.40	10.38	1.22	12.53	21.01	0.61	0.00	99.24
51.39	0.36	2.42	9.91	0.67	12.87	22.30	0.85	0.00	100.77
51.47	0.61	2.86	7.54	0.24	14.65	21.99	0.47	0.00	99.82
Post-CI samples									
50.19	0.41	2.36	13.01	1.42	10.97	21.73	0.47	0.00	100.56
49.41	1.03	2.58	12.51	1.12	11.01	20.30	0.84	0.00	98.80
50.01	0.78	3.28	10.04	0.43	12.48	22.28	0.62	0.00	99.92
49.26	1.06	3.97	8.61	0.33	13.43	22.07	0.57	0.00	99.30
50.29	0.30	2.53	9.54	0.89	14.03	21.78	0.23	0.00	99.59
50.00	0.25	3.03	8.37	0.61	13.58	22.46	0.38	0.00	98.68
50.76	0.72	2.06	11.46	1.41	11.22	20.07	0.96	0.00	98.66
51.06	0.72	1.63	12.50	1.13	11.86	20.88	0.65	0.00	100.43
51.01	0.47	1.13	11.22	1.06	11.85	21.12	0.74	0.00	98.60
50.93	0.76	1.28	11.37	1.50	11.49	21.80	0.77	0.00	99.90
Plagioclase Compositions - in Weight Percent									
Pre-CI samples									
64.45	0.27	18.97	0.00	0.00	0.00	0.76	4.36	11.20	100.01
62.05	0.32	19.27	0.18	0.91	0.19	0.85	4.83	11.39	99.99
62.53	0.64	19.44	0.00	0.00	0.01	0.79	4.36	12.16	99.93
62.01	0.00	20.17	0.41	0.00	0.00	0.45	4.54	12.10	99.68
64.50	0.00	19.09	0.00	0.13	0.00	0.45	4.00	11.82	99.99
63.05	0.00	18.93	0.64	0.00	0.25	0.63	4.29	12.20	99.99
61.44	0.00	19.87	0.73	0.00	0.16	1.51	4.44	11.85	100.00
62.25	0.14	18.89	0.86	0.00	0.00	0.82	4.50	12.54	100.00
61.52	0.26	19.59	1.06	0.00	0.11	0.44	4.29	12.60	99.87
62.22	0.00	20.04	0.09	0.70	0.00	0.37	4.54	12.04	100.00
CI samples									
63.12	0.00	19.08	0.00	0.28	0.00	0.60	4.17	11.35	98.60
62.66	0.18	18.93	1.74	0.00	0.00	1.03	4.37	11.60	100.51
62.10	0.46	19.07	0.00	0.59	0.05	0.15	4.19	11.47	98.08
64.78	0.00	18.47	0.04	0.00	0.00	0.56	4.22	12.58	100.65
61.41	0.17	19.69	0.00	0.81	0.27	0.56	3.96	12.06	98.93
61.27	0.06	19.42	1.25	0.39	0.12	0.54	4.06	12.46	99.57
61.74	0.00	19.06	0.00	0.88	0.23	0.92	4.19	11.94	98.96
62.40	0.36	19.67	0.00	0.00	0.00	0.89	4.84	12.62	100.78
62.35	0.67	18.73	0.50	0.06	0.10	0.53	4.41	12.39	99.74
62.98	0.00	17.81	0.00	0.00	0.00	1.47	4.10	12.59	98.95
Post-CI samples									
62.62	0.53	19.03	0.00	0.00	0.45	0.47	2.32	14.59	100.01
62.96	0.00	18.74	0.00	0.00	0.40	0.46	2.40	15.03	99.99

63.61	0.32	18.71	1.64	0.24	0.48	2.23	4.02	8.70	0.06	100.00	60.94	0.30	19.25	0.40	0.00	0.02	0.71	2.41	15.93	99.96
64.80	0.55	17.37	1.36	0.47	0.50	1.86	4.30	8.78	0.00	100.00	61.72	0.16	18.80	0.08	0.94	0.00	0.60	2.84	14.40	99.54
63.59	1.05	18.69	2.02	0.00	0.35	1.99	4.50	7.81	0.00	100.00	62.00	0.43	18.02	0.00	0.29	0.04	1.04	2.84	15.33	99.99
62.53	0.53	19.01	2.79	0.00	0.28	2.09	4.39	8.38	0.00	100.00	62.86	0.22	18.68	0.86	0.00	0.00	0.25	2.57	14.57	100.01
62.47	0.50	18.77	3.41	0.02	0.25	2.15	4.02	8.40	0.00	100.00	62.77	0.09	18.52	0.00	0.00	0.02	0.70	2.37	15.44	99.91
63.38	0.37	17.17	3.18	0.49	0.43	1.70	4.59	8.69	0.00	100.00	61.24	0.00	18.56	0.00	0.55	0.00	0.90	2.51	15.12	98.88
61.95	0.64	17.67	3.14	0.00	0.71	2.36	4.70	8.83	0.00	100.00	60.89	0.00	19.53	1.53	0.42	0.00	0.33	2.64	14.66	100.00
62.28	0.63	18.35	2.57	0.27	0.45	2.22	4.36	8.86	0.00	100.00	62.94	0.45	18.68	0.56	0.00	0.00	0.57	2.58	14.16	99.94